Research Article | Vol. 11, No. 10 / 1 October 2020 / Biomedical Optics Express 5814
Biomedical Optics EXPRESS

Moxifloxacin based fluorescence imaging of intestinal goblet cells

SEUNGHUN LEE,[1,6] SEONGHAN KIM,[1,6] KWANGWOO NAM,[2] SUN YOUNG KIM,[3] SEUNGRAG LEE,[4] SEUNG-JAE MYUNG,[3,7] AND KI HEAN KIM[1,5,8]

[1]*Department of Mechanical Engineering, Pohang University of Science and Technology, 77 Cheongam-ro, Nam-gu, Pohang, Gyeongbuk 37673, South Korea*
[2]*Department of Internal Medicine, Dankook University College of Medicine, 201 Manghyang-ro, Dongnam-gu, Cheonan, Chungnam 31116, South Korea*
[3]*Department of Gastroenterology, Digestive Diseases Research Center, Asan Institute for Life Sciences, Asan Medical Center, University of Ulsan College of Medicine, 88 Olympic-ro, 43-gil, Songpa-gu, Seoul 05505, South Korea*
[4]*Medical Device Development Center, Osong Medical Innovation Foundation, 123 Osongsaengmyeong-ro, Heungdeok-gu, Cheongju, Chungbuk 28160, South Korea*
[5]*Division of Integrative Biosciences and Biotechnology, Pohang University of Science and Technology, 77 Cheongam-ro, Nam-gu, Pohang, Gyeongbuk 37673, South Korea*
[6]*These authors contributed equally to this work*
[7]*sjmyung@amc.seoul.kr*
[8]*kiheankim@postech.ac.kr*

Abstract: Goblet cells (GCs) in the intestine are specialized epithelial cells that secrete mucins to form the protective mucous layer. GCs are important in maintaining intestinal homeostasis, and the alteration of GCs is observed in inflammatory bowel diseases (IBDs) and neoplastic lesions. In the Barrett's esophagus, the presence of GCs is used as a marker of specialized intestinal metaplasia. Various endomicroscopic imaging methods have been used for imaging intestinal GCs, but high-speed and high-contrast GC imaging has been still difficult. In this study, we developed a high-contrast endoscopic GC imaging method: fluorescence endomicroscopy using moxifloxacin as a GC labeling agent. Moxifloxacin based fluorescence imaging of GCs was verified by using two-photon microscopy (TPM) in the normal mouse colon. Label-free TPM, which could visualize GCs in a negative contrast, was used as the reference. High-speed GC imaging was demonstrated by using confocal microscopy and endomicroscopy in the normal mouse colon. Confocal microscopy was applied to dextran sulfate sodium (DSS) induced colitis mouse models for the detection of GC depletion. Moxifloxacin based GC imaging was demonstrated not only by 3D microscopies but also by wide-field fluorescence microscopy, and intestinal GCs in the superficial region were imaged. Moxifloxacin based endomicroscopy has a potential for the application to human subjects by using FDA approved moxifloxacin.

© 2020 Optical Society of America under the terms of the OSA Open Access Publishing Agreement

1. Introduction

Goblet cells (GCs) in the intestinal tract are specialized epithelial cells, responsible for the production and maintenance of protective mucus blanket by secreting high-molecular-weight glycoproteins known as mucins. The mucus layer protects the underlying epithelium against luminal contents such as digestive enzymes, microbes and microbial products [1], and GCs modulate their mucin secretion in response to external stimuli [2]. GCs play an important role in adaptive immunity as well by functioning as an antigen-presenting pathway to underlying dendritic cells in response to the luminal environment [3]. Therefore, in-vivo GC imaging in the intestinal tract will be useful for studying physiological and immunological responses to various

#402350 https://doi.org/10.1364/BOE.402350
Journal © 2020 Received 9 Jul 2020; revised 3 Sep 2020; accepted 7 Sep 2020; published 23 Sep 2020

Biomedical Optics EXPRESS

enteric stimulations in biology. GC alteration and dysfunction are associated with mucosal diseases such as inflammatory bowel diseases (IBDs). The population of GCs decreases in ulcerative colitis (UC) due to defective maturation, while it is maintained in Crohn's disease with inflammation stimulation [4]. Although GC alteration happens in different directions depending on the disease type, GC alteration could be used for the detection of the neoplastic lesions in patients with longstanding UC [5]. In the esophagus, GC imaging is important for detecting specialized intestinal metaplasia [6]. Specialized intestinal metaplasia can be an indicator of potential malignant progression to esophagus adenocarcinoma, and the appearance of GCs in the epithelium is a histopathological criterion of specialized intestinal metaplasia owing to its transformation from the squamous epithelium into the intestinal resembling epithelium [7].

High-resolution endomicroscopy techniques have been used for imaging intestinal GCs during endoscopic surveillance. Confocal laser endomicroscopy (CLE) is a widely used technique with the availability of commercial products, and CLE with the intravenous injection of fluorescein visualized GCs and other cells in negative contrasts [8]. CLE detected neoplastic lesions in the colon of longstanding UC patients based on the absence of GCs and other biomarkers [5], and detected specialized intestinal metaplasia in Barrett's esophagus based on the presence of GCs [9]. Label-free two-photon microscopy (TPM), a 3D imaging technique based on auto-fluorescence (AF) of cells, was used for the ex-vivo examination of freshly excised gastric and intestinal tissues [10–12]. Label-free TPM visualized GCs in a negative contrast owing to the absence of AF in the mucins inside GC cytoplasm, and detected intestinal metaplasia in ex-vivo gastric tissues based on the presence of GCs. However, label-free TPM has limitations in the slow imaging speed and high technical difficulty for endomicroscopy implementation. Optical coherence microscopy (OCM) and spectrally encoded confocal microscopy (SECM) are high-resolution high-speed 3D imaging techniques based on light reflection, and they have been used for non-invasive GC imaging in gastroesophageal and intestinal tissues [13–19]. OCM and SECM visualized GCs in negative contrasts owing to relatively low reflectivity, associated with their translucent mucin contents. OCM and SECM identified specialized intestinal metaplasia in gastroesophageal junction by visualizing GCs. OCM and SECM have advantages in GC detection by providing comprehensive endoscopic surveillance with high-speed imaging but have limitations of low image contrasts and no molecular specificity. Although these microscopic and endomicroscopic techniques could detect GCs, they visualized GCs in negative contrasts. An endomicroscopic technique visualizing GCs in a positive contrast would be useful for the more sensitive detection.

Recently we developed a high-contrast cell imaging method in biological tissues, and it was fluorescence microscopy using moxifloxacin as a cell labeling agent [20–22]. Moxifloxacin is an antibiotic used in both the treatment and prevention of ocular and other infections. Moxifloxacin has intrinsic fluorescence [23] and good pharmacokinetic properties for tissue penetration [24]. Moxifloxacin labeling of cells was conducted via topical administration of moxifloxacin ophthalmic solution and short time incubation, and fluorescence microscopy techniques such as confocal microscopy (CM) and TPM were used for high-contrast cell imaging within tissues. Moxifloxacin labeled all the cells within tissues without specification, but some cells were labeled more strongly than others. These cells were Paneth cells in the small intestine [25] and GCs in the conjunctiva [26]. Moxifloxacin appeared to label secretive cells especially well, although the mechanism needs to be studied further.

In this study, moxifloxacin based fluorescence microscopy and endomicroscopy were tested in the imaging of intestinal GCs. TPM was used for the verification of moxifloxacin based imaging of GCs in the mouse colon in comparison with label-free TPM as the reference. Then, CM and CLE were used for high-speed and large-sectional imaging of GCs in the mouse colon, *in vivo*. CM was applied to dextran sulfate sodium (DSS) induced colitis mouse models for the detection of GC depletion. Wide-field fluorescence microscopy (WFFM) of intestinal GCs was demonstrated.

Biomedical Optics EXPRESS

2. Methods

2.1. Two-photon and confocal microscopy system

A commercial laser scanning microscopy system (SP-5, Leica), which has dual functionalities of TPM and CM, was used for the 3D imaging of intestinal GCs in the mouse colon. In the case of TPM, a Ti:sapphire femtosecond laser (Chameleon Vision, Coherent Inc.) with 140 femtosecond pulse width, 80 MHz repetition rate and the tunable wavelength from 680 nm to 1080 nm was employed as the excitation light source. The excitation wavelength was tuned at 780 nm for both label-free and moxifloxacin based TPM. Fluorescence light from the sample was collected at a single channel in the spectral range from 455 nm to 655 nm. In the case of CM, a 405 nm laser diode was used for the one-photon excitation of moxifloxacin. Fluorescence light from the sample was de-scanned and collected at a single channel in the wavelength range from 455 nm to 665 nm. A 20x objective lens (Water immersion, NA 1.0, HCX APO L, Leica) was used for both the TPM and CM imaging.

2.2. Confocal laser endomicroscopy system

A custom-built CLE system was used for the imaging of intestinal GCs in the mouse colon, *in vivo*. A schematic of the CLE system is shown in Fig. 1(a). The system was the combination of a confocal miniprobe (Gastroflex UHD, Mauna Kea Technology) and a high-speed confocal microscope. The miniprobe has the field of view (FOV) of 240 μm in diameter, the lateral resolution of 1 μm, the confocal depth of 55-65 μm from the distal probe surface. The miniprobe was added onto the confocal microscope, by placing its proximal end in the focal plane of an objective lens in the confocal microscope. The confocal microscope used a 405 nm diode laser (MDL-III-405-100mW, Changchun New Industries Optoelectronics technology) as the excitation light source. Excitation light from the source was first reflected on a dichroic mirror (T430LPXR, Chroma Technology) which separated excitation and emission light, and then reflected on the combination of a resonant scanner (CRS 8 KHz, Cambridge Technology) and a galvanometer (6220H, Cambridge technology). Excitation light after the scanner went through the combination of a scan lens (AC254-50-A, Thorlabs) and a tube lens (AC508-200-A, Thorlabs) and to a 10x objective lens (Multi immersion, NA 0.4, HC PL APO, Leica). The objective lens focused excitation light onto the proximal end of the confocal miniprobe. Glycerol was used as an immersion medium between the objective lens and the miniprobe. Coupled excitation light into the miniprobe was delivered to the distal end and focused into the specimen. The scanner combination scanned the excitation focus across the specimen. Fluorescence light from the specimen was collected back by the miniprobe, delivered to its proximal end and coupled into the microscope. Fluorescence light delivered back to the scanner was de-scanned, transmitted through the dichroic mirror and an emission filter (ET525/70 M-2P, Chroma Technology), and then focused at a pinhole (P50D, Thorlabs) by an achromatic lens (AC254-40-A, Thorlabs). Fluorescence light transmitted through the pinhole was collected at a photomultiplier tube (H10770A-40, Hamamatsu). Fluorescence was detected in a single detection channel in the spectral range from 490 nm to 560 nm with the emission filter. The spectral range was chosen to reduce AF in the confocal miniprobe at 405 nm excitation (Fig. S1 in Supplement 1). Imaging parameters of the CLE system were determined by those of the miniprobe.

2.3. Wide-field fluorescence microscopy system

A custom-built WFFM system was used for the imaging of intestinal GCs in the mouse colon, *in vivo*. A schematic of the WFFM system is shown in Fig. 1(b). A light emitting diode with the center wavelength at 405 nm (M405L4, Thorlabs) was employed as the excitation light source. The excitation light was spectrally filtered by an excitation filter (ZET405/20x, Chroma Technology), reflected by a dichroic mirror (T425LPXR-UF1, Chroma Technology) and delivered

Biomedical Optics EXPRESS

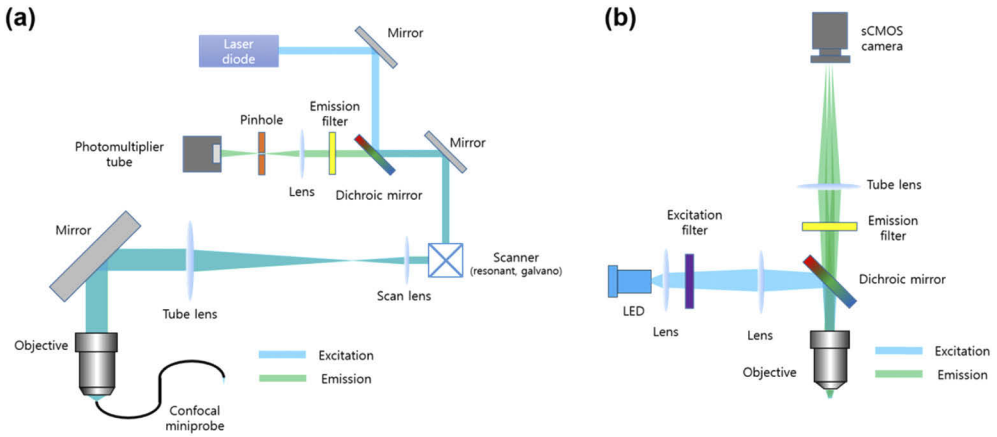

Fig. 1. Schematics of a confocal laser endomicroscopy system (a) and a wide-field fluorescence microscopy system (b), which were used for the imaging of intestinal goblet cells.

to a 10x objective lens (Dry, NA 0.25, Plan N, Olympus). The objective lens illuminated the sample uniformly. Fluorescence light from the sample was collected by the same objective lens, transmitted through the dichroic mirror and a barrier filter (ET430LP, Chroma technology), and imaged at a sCMOS camera (4.2 edge, PCO) with a tube lens (AC254-200-A, Thorlabs). The maximum imaging speed was 40 frames/s, determined by the camera. The WFFM system had 1.5 μm transverse resolution and 30 μm depth of field, determined by the camera.

2.4. Sample preparation

All animal procedures in this study were approved by the Institutional Animal Care and Use Committee (POSTECH-2019-0061). 5~7 weeks balb/c mice kept under specific pathogen-free conditions at the POSTECH Biotech Center were used for both the ex-vivo and in-vivo intestinal GC imaging. Colitis was induced by adding 2% DSS (w/v) to drinking water for 6 days, and then DSS-free water was provided for 1 day. 7 mice in total (5 normal and 2 colitis models) were used in the experiments.

2.5. Ex-vivo imaging of the normal mouse colon with both label-free and moxifloxacin based two-photon microscopy

For the collection of fresh colon tissues, mice were humanely euthanized. The abdominal side was surgically opened, and a part of the colon was excised and was longitudinally cut to expose the luminal side. The colon specimens were flattened on slide glasses, and then label-free TPM was conducted. After the label-free TPM imaging, a FDA approved moxifloxacin ophthalmic solution (Vigamox, Alcon) containing 12.4 mM of moxifloxacin hydrochloride was topically administered on the colon specimens and left for 5 min. The colon specimens were washed with phosphate buffered saline (PBS) and moxifloxacin based TPM was conducted. The FOV for both label-free and moxifloxacin based TPM was 194 μm x 194 μm with 512 pixels × 512 pixels, and their 3D imaging was conducted by translating the objective in the depth direction with 2 μm step size. In the label-free TPM, the imaging speed was 0.14 frames/s, and the excitation power was 71 mW approximately. In the moxifloxacin based TPM, 11 mW excitation power was used, and the imaging speed was 0.4 frames/s.

Biomedical Optics EXPRESS

2.6. In-vivo imaging of the mouse colon with moxifloxacin based confocal microscopy, confocal laser endomicroscopy and wide-field fluorescence microscopy

All the in-vivo imaging of mouse colon was conducted under anesthesia. Mice were anesthetized with a gas mixture of 15%/vol isoflurane (Terrell, Piramal Critical Care) and oxygen gas. An incision was made on the abdominal skin to access the colon, and the colon was pulled out from the abdominal cavity and mounted on a custom-built intestinal holder (Live Cell Instrument Inc). The colon was cut open in the longitudinal direction for the exposure of the luminal side, and the moxifloxacin ophthalmic solution containing 12.4 mM of moxifloxacin hydrochloride was topically administered and left for 5 min. The colon was washed with PBS and moxifloxacin based fluorescence imaging on the luminal side was conducted. The body temperature was maintained at 37 °C by using a heating pad in the intestine holder. After the imaging, mice were euthanized immediately.

In the case of CM, the imaging speed was 29.4 frames/s, and the FOV was 369 μm x 369 μm with 512 pixels × 512 pixels. Volumetric imaging was conducted by axially translating the objective from the surface with 1 μm step size. Excitation power was 2.3 mW. In the case of CLE, the imaging speed and FOV were 15 frames/s and 240 μm in diameter. Excitation power was less than 1 mW. Honeycomb pattern in the CLE images, which was an artifact of the miniprobe, was removed by using the iterative shrinkage thresholding algorithm [27]. In the case of WFFM, the imaging speed was 40 frames/s and FOV was 1.2 mm x 1.2 mm. Excitation power was 6 mW.

2.7. Histological examination

The colon specimens, which were imaged in fresh condition, were fixed with 4% formaldehyde for 24~48 h, embedded in paraffin, and sectioned in 5 μm thickness. Tissues on slides were stained with hematoxylin and eosin (H&E) for 30 s, respectively. Serial sectioned tissue slides were deparaffinized in xylene, rehydrated in 70, 80, 90, 95, and 100% alcohol for 5 min, and washed with distilled water. The hydrated slides were stained with Periodic Acid solution and Schiff's (PAS) reagent to image GCs under an examination microscope.

3. Results

3.1. Verification of moxifloxacin based fluorescence imaging of intestinal goblet cells in the mouse colon

Moxifloxacin based fluorescence imaging of intestinal GCs was tested by using TPM in the mouse colon (Fig. 2). TPM was used in this experiment for the comparison of moxifloxacin based TPM with label-free TPM which was used for intestinal GC imaging previously [10–12]. Label-free TPM visualized GCs in a negative contrast owing to the lack of AF in the mucins inside GC cytoplasm. TPM imaged ex-vivo mouse colon specimens twice, once before the topical administration of moxifloxacin ophthalmic solution for label-free imaging and then after the moxifloxacin administration. The two TPM images were compared side by side. In the label-free TPM images, GCs appeared dark compared to the surrounding epithelial cells owing to different AF expression (Fig. 2(a)-(c)). On the other hand, GCs were visualized bright in the moxifloxacin based TPM images compared to the surrounding epithelial cells via moxifloxacin labeling (Fig. 2(d)-(f)). The two TPM images showed good spatial co-registration, even though these images were acquired sequentially. The two TPM images were displayed in different colormaps and were merged. In the merged TPM images, GCs and other epithelial cells appeared in different colors owing to the different color combinations (Fig. 2(g)-(k)). The bright cells in the moxifloxacin based TPM images were spatially co-registered with dark ones in the label-free TPM images, and this confirmed the moxifloxacin based fluorescence imaging of GCs in the mouse colon.

Biomedical Optics EXPRESS

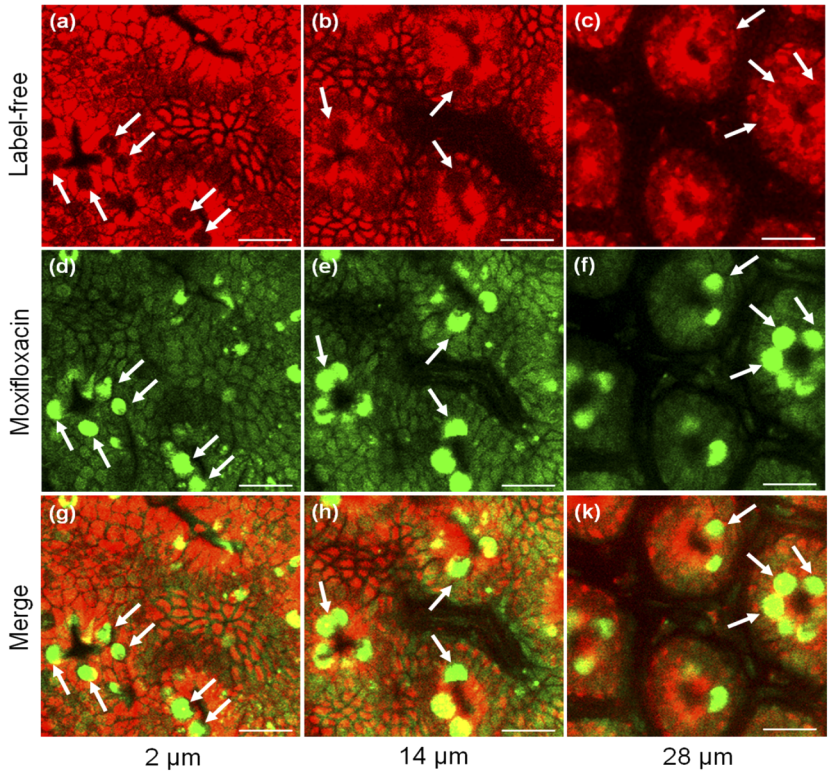

Fig. 2. Verification of moxifloxacin based two-photon microscopy (TPM) imaging of intestinal goblet cells in the ex-vivo mouse colon in comparison with label-free TPM. (a-c) and (d-f) : label-free TPM and moxifloxacin based TPM images at 3 different depths (2 μm, 14 μm and 28 μm), scale bars 20 μm, (g-k) : co-registered images of label-free TPM and moxifloxacin based TPM, scale bars 20 μm. Arrows mark goblet cells which appeared in a negative and a positive contrast in the label-free TPM and the moxifloxacin based TPM images, respectively.

Signal to background ratio (SBR) of intestinal GCs in the moxifloxacin based TPM images was analyzed. Regions of intestinal GCs and other cells in the crypt image were automatically segmented by using the Otsu thresholding method (Fig. S2 in Supplement 1), and average intensities of the two regions were calculated. The SBR of intestinal GCs was obtained as the ratio of fluorescence intensities of intestinal GCs and other cells in the crypts. 30 intestinal crypts in total were used in the SBR analysis, and the average SBR of intestinal GCs was 3.9 ± 0.4.

3.2. *High-speed intestinal goblet cell imaging by using moxifloxacin based confocal microscopy and endomicroscopy in the normal mouse colon, in vivo*

Although moxifloxacin based intestinal GC imaging was confirmed and by using TPM, TPM was not an optimal method due to its low two-photon excitation efficiency and technical difficulties in endomicroscopy implementation. CM and CLE were used instead for the high-speed GC imaging and examination, and CM could image GCs in the superficial regions down to approximately 50 μm deep from the surface. The results of high-speed GC imaging in the normal mouse colon by moxifloxacin based CM and CLE are shown in Fig. 3. The imaging speed of CM was approximately 30 frames/s (see **Visualization 1**), and large sectional images were generated by conducting high-speed 3D imaging with sample translation and mosaicking. A representative

Biomedical Optics EXPRESS

large-sectional mosaic image of intestinal GCs is presented in Fig. 3(a). The mosaic image had the FOV of 1.3 mm x 1 mm via the combination of 4×3 individual images. The mosaic image showed the distribution of GCs in the normal mouse colon at 25 μm deep from the luminal surface. GCs were mainly found within crypts so that the distribution of crypts could be inferred from the GC images. GCs and GC containing crypts were uniformly distributed in the normal mouse colon. There were regions with no GC in the mosaic image, and such regions were caused not by the absence of GC but by the irregular tissue surface. The luminal surface in those regions was too low compared to the surrounding, and the objective lens mounted on a translator with 200 μm working distance could not reach the surface. A boxed region with red lines in the mosaic image was magnified to show intestinal GCs in detail. An en-face image and a corresponding cross-sectional image are presented in Fig. 3(b) and 3(c), respectively. The magnified en-face image showed radially distributed GCs in the crypts and the cross-sectional image showed the axial distribution of GCs in the crypts. Corresponding H&E and PAS histological images revealed the regular distribution of GCs in the normal mouse colon (Fig. 3(d)-(e)). The number of GCs per crypt within the imaging depth of 50 μm was 8.3 ± 1.9 ($n = 30$) from the CM images.

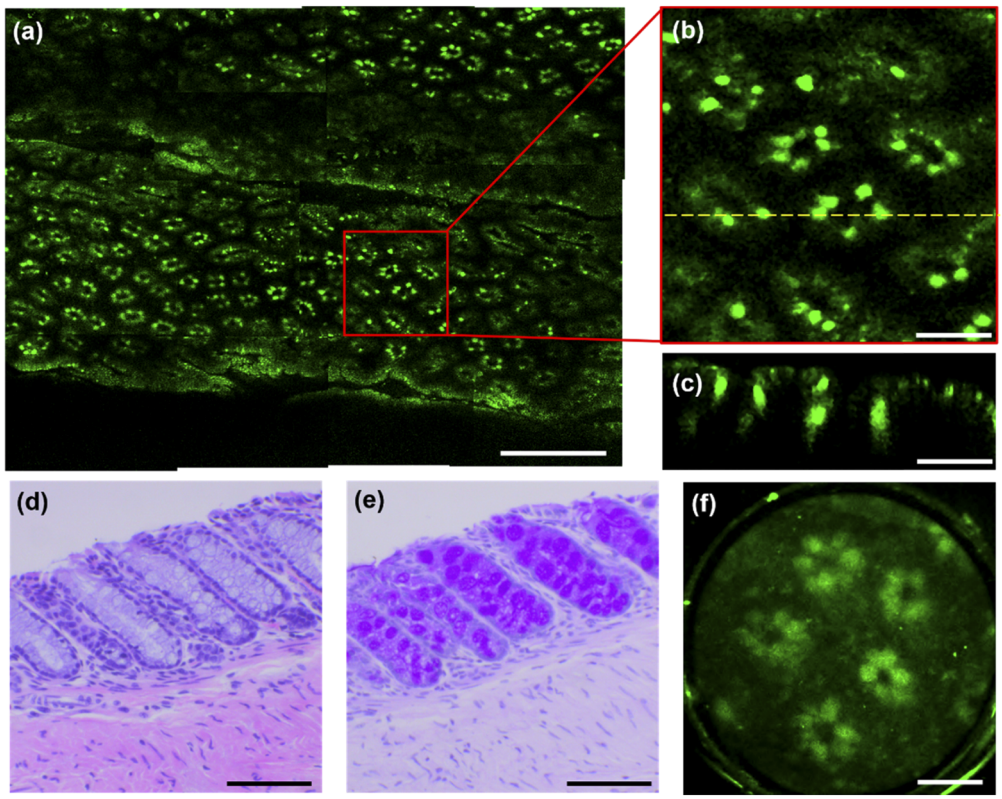

Fig. 3. Moxifloxacin based confocal microscopy and endomicroscopy images of the normal mouse colon, *in vivo*. (a): a large sectional image showing the luminal side of the mouse colon, scale bar 300 μm. (b) and (c): a magnified image of the marked region in the large sectional image and a cross-sectional image, scale bars 50 μm, a yellow dot line indicates the plane of the cross-sectional image. (d) and (e): Hematoxylin & Eosin and Periodic Acid Schiff histology images, scale bars 100 μm. (f): a confocal endomicroscopy image on the luminal side, scale bar 50 μm.

In-vivo moxifloxacin based CLE imaging of intestinal GCs in the normal mouse colon was also demonstrated (Fig. 3(f) and see **Visualization 2**). The imaging depth was approximately 25

Biomedical Optics EXPRESS

μm deep from the surface to capture crypts below the surface. CLE visualized GC clusters within crypts similarly to CM with slight degradation in the image resolution. The image resolution of CLE was 1 μm and 10 μm in the transverse and axial directions respectively, while the one of CM was 0.2 μm and 0.8 μm, respectively. GCs were visualized by both CM and CLE in high contrasts via moxifloxacin labeling.

3.3. *Moxifloxacin based confocal microscopy of the colon in colitis mouse models, in vivo*

Moxifloxacin based CM imaging of intestinal GCs was conducted in the colon of DSS induced colitis mouse models, *in vivo* (Fig. 4). DSS induced colitis mouse model is a well-known chemically induced colitis model with the depletion of GCs in severe cases [28,29], and moxifloxacin based CM was tested for detecting GC depletion. Large sectional images were generated by high-speed CM imaging with sample translation and mosaicking. A representative en-face mosaic image of the colitis mouse colon is shown in Fig. 4(a). Fluorescence levels in the colitis colon image were quite low compared to those in the normal colon image. Not many cells were visible except some scattered bright cells. Crypts were barely visible due to low fluorescence levels. A magnified image from the red boxed region in the mosaic image and a

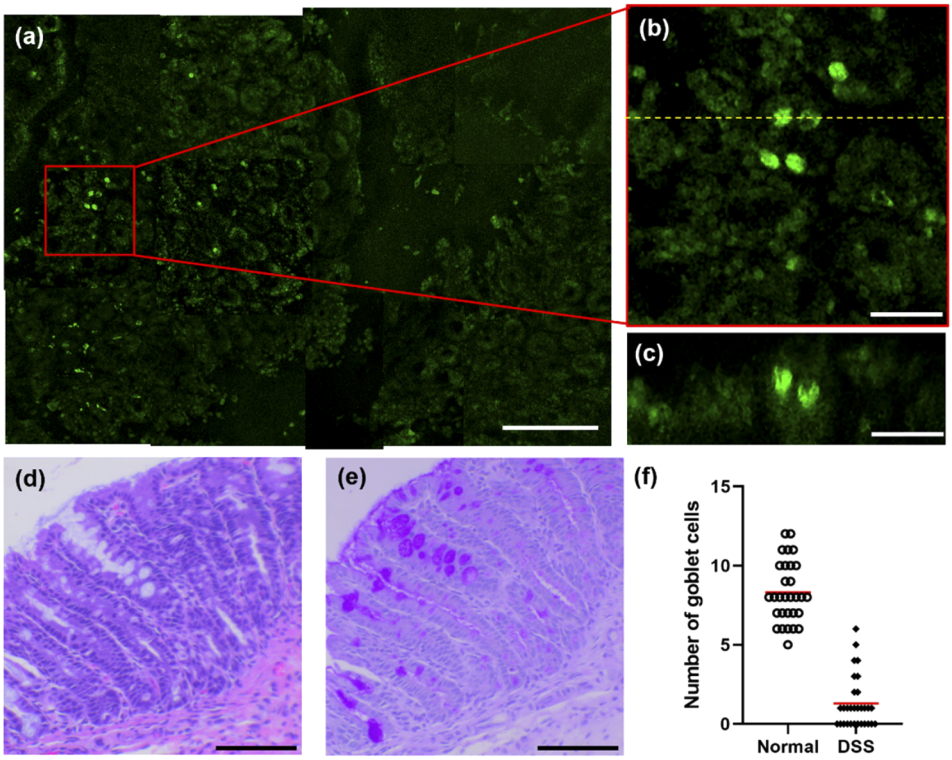

Fig. 4. Moxifloxacin based confocal microscopy images of the dextran sulfate sodium (DSS) induced colitis mouse colon, *in vivo*. (a) : a large sectional image showing the luminal side of mouse colon, scale bar 300 μm. (b) and (c): a magnified image of the marked region in the large sectional image and a cross-sectional image, scale bars 50 μm, a yellow dot line indicates the plane of the cross-sectional image. (d) and (e) : Hematoxylin & Eosin and Periodic Acid Schiff histology images, scale bars 100 μm. (f) : the number of goblet cells per crypt within 50 μm depth from the luminal surface.

Biomedical Optics EXPRESS

corresponding cross-sectional image showed more detailed cellular structures. (Figure 4(b)-(c)). Most cells within and outside the crypts expressed low fluorescence intensities. There were only a few cells expressing strong fluorescence in the magnified image, indicating the depletion of intestinal GCs. GC depletion was confirmed with corresponding histology images (Fig. 4(d)-(e)). The number of GCs per crypt within the imaging depth of 50 µm, calculated from the CM images of DSS induced colitis colon, was 1.3 ± 1.6 (n=30). Even though some crypts had several GCs, most crypts had no or only one GC. Compared to the normal colon, the number of GCs was significantly reduced (Fig. 4(f)).

3.4. *Moxifloxacin based wide-field fluorescence microscopy of the colon in both normal and colitis mouse models, in vivo*

3D fluorescence microscopy techniques including TPM and CM demonstrated high-contrast intestinal GC imaging in the mouse colon with moxifloxacin labeling. GCs appeared bright compared to other cells in the 3D images with moxifloxacin labeling. Because moxifloxacin based fluorescence imaging visualized GCs in a positive contrast, WFFM could be used for imaging GCs on the surface. WFFM does not have 3D resolution and may visualize GCs in the superficial region only in focus, but WFFM is much simpler and could be faster than 3D microscopic methods for endomicroscopic imaging. As the first step, WFFM was used to image the exposed lumen of the mouse colon in both normal and DSS colitis mouse models (Fig. 5).

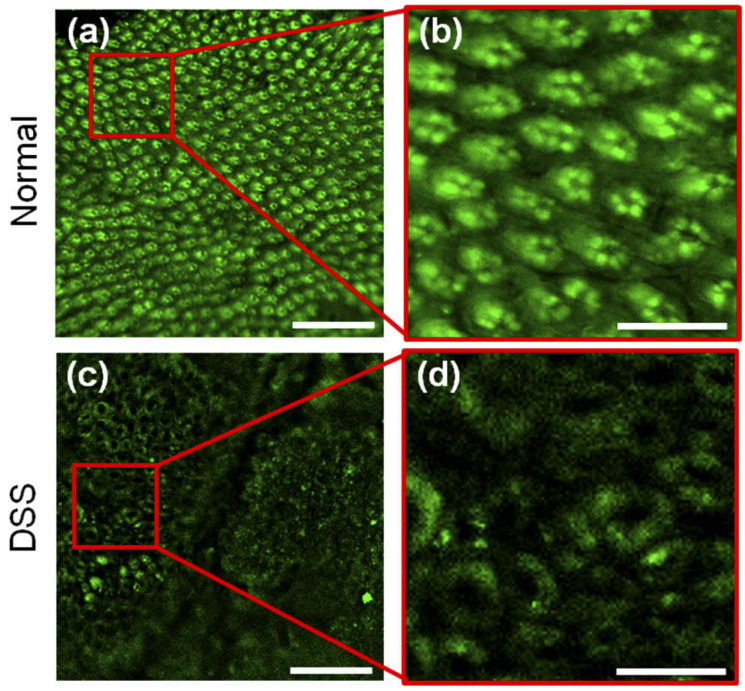

Fig. 5. Moxifloxacin based wide-field fluorescence microscopy (WFFM) images of the normal and dextran sulfate sodium (DSS) induced colitis mouse colon, *in vivo*. (a): a moxifloxacin based WFFM image showing the luminal side of normal mouse colon, scale bar 300 µm. (b): a magnified image of the marked region in the moxifloxacin based WFFM image of normal mouse colon, scale bar 100 µm. (c): a moxifloxacin based WFFM image showing the luminal side of DSS induced colitis mouse colon, scale bar 300 µm. (d): a magnified image of the marked region in the moxifloxacin based WFFM image of DSS induced colitis mouse colon, scale bar 100 µm.

Biomedical Optics EXPRESS

WFFM could visualize GCs within crypts similarly to CM and CLE, although the WFFM images had relatively low image resolutions and relatively high backgrounds. WFFM was designed to have the relatively low magnification of 10x and the numerical aperture (NA) of 0.25 to increase the FOV and the depth of field. A WFFM image in the full FOV showed uniformly distributed GCs in the normal mouse colon (Fig. 5(a)). The FOV of WFFM was 1.2 mm x 1.2 mm, 3.3 times larger than the one of CM. A magnified WFFM image of the normal mouse colon showed GCs in the crypts (Fig. 5(b)). Individual GCs were clearly visualized, although there were some background intensities partly due to the lack of 3D sectioning capability and the relatively low NA of the current WFFM. WFFM images of the DSS induced colitis mouse colon (Fig. 5(c)-(d)) showed the depletion of GCs and low fluorescence intensities similarly to the results of CM. These WFFM results showed the potential for simple endomicroscopy.

4. Discussion and conclusion

A high-contrast endoscopic intestinal GC imaging method was developed. Moxifloxacin ophthalmic solution was used for labeling intestinal GCs via topical administration, and fluorescence microscopies and endomicroscopy could visualize GCs in the positive contrast. Moxifloxacin based fluorescence imaging of intestinal GCs was verified by label-free TPM which visualized GCs in the negative contrast. The mechanism of moxifloxacin labeling of GCs needs to be elucidated further, but moxifloxacin seems to label secretive cells including Paneth cells in the small intestine and GCs in the conjunctiva and intestinal tract. High-speed intestinal GC imaging was demonstrated by CM and CLE. Video-rate imaging was possible with the excitation energy of 0.87 J/cm^2, which was much less (approximately 62 times less) than the damage threshold [30]. The regular distribution of GCs in the normal mouse colon and the depletion of GCs in the colon of DSS induced colitis mouse models were visualized. The previous GC imaging methods including fluorescein based CLE, label-free TPM, and reflection based OCM and SECM visualized GCs in the negative contrasts. However, moxifloxacin based fluorescence imaging could visualize GCs in the positive contrast. GC imaging was possible not only by 3D microscopies but also by WFFM without 3D resolution, although GCs in the superficial region of the colon were visualized. Endoscopy development of moxifloxacin based WFFM would be straightforward.

Moxifloxacin ophthalmic solution was used to label intestinal GCs in the colon via topical administration and short time incubation of several minutes. Therefore, moxifloxacin solution could be sprayed onto the lumen through the instrumentation channel of clinical endoscopes and an endomicroscope could be introduced through the same channel afterward. The possibility of photodamage by excitation light is low by using much less energy than the damage threshold. Moxifloxacin based endomicroscopic imaging can be applicable to human subjects, because moxifloxacin ophthalmic solution is FDA approved for the treatment and prevention of bacterial infection in the human eye. However, the application of moxifloxacin ophthalmic solution to the endoscopic imaging of intestinal tracts need to be tested and approved before the human applications. Moxifloxacin could be used together with other fluorescent agents such as fluorescein for the better visualization. The combination of moxifloxacin and fluorescein could be useful for the enhanced visualization of cellular structures in the gastrointestinal tract. Fluorescence of the two fluorescent agents could be separated owing to their different excitation spectra: from 270 nm to 405 nm and from 475 nm to 525 nm for moxifloxacin and fluorescein, respectively. The next step of moxifloxacin based fluorescence endomicroscopy could be in-vivo GC imaging in large animal models such as swine models and ex-vivo imaging of patient specimens such as specialized intestinal metaplasia specimens in the esophagus and metaplastic lesions in the colon.

In conclusion, a high-contrast endoscopic intestinal GC imaging method was developed by using moxifloxacin as the labeling agent and fluorescence microscopic/endomicroscopic techniques. CM and CLE showed the high-speed imaging of GCs in the normal mouse colon,

Biomedical Optics EXPRESS

and CM demonstrated the detection of GC depletion in the DSS colitis mouse model. Simple WFFM could be used for GC imaging in the superficial region. The new high-contrast intestinal GC imaging method has potentials for the endoscopic examination of GC alteration and the detection of associated diseases by using the FDA approved moxifloxacin as the labeling agent.

Funding

National Research Foundation of Korea (2020R1A2C3009309, 2017R1A2A1A18070960); Ministry of Science and ICT and Future Planning of Korea government (NRF-2017M3C7A 1044964); Institute of Information & communications Technology Planning & Evaluation (TTIP) of Korea Government (No.2020-0-00989); Ministry of Health & Welfare of Korea government (Collaborative research supporting program).

Acknowledgments

The authors give thanks to Kyuseop Cho who manages and operates the commercial laser scanning microscopy system.

Disclosures

SL, SK, SL, SJM and KHK are authors of a patent filed for moxifloxacin based endoscopic imaging of intestinal goblet cells.

See Supplement 1 for the supporting content (Fig. S1 and Fig. S2).

References

1. C. Laboisse, A. Jarry, J. E. Branka, D. Merlin, C. Bou-Hanna, and G. Vallette, "Recent aspects of the regulation of intestinal mucus secretion," Proc. Nutr. Soc. **55**(1B), 259–264 (1996).
2. P. Dharmani, V. Srivastava, V. Kissoon-Singh, and K. Chadee, "Role of Intestinal Mucins in Innate Host Defense Mechanisms against Pathogens," J. Innate Immun. **1**(2), 123–135 (2009).
3. J. R. McDole, L. W. Wheeler, K. G. McDonald, B. Wang, V. Konjufca, K. A. Knoop, R. D. Newberry, and M. J. Miller, "Goblet cells deliver luminal antigen to CD103+ dendritic cells in the small intestine," Nature **483**(7389), 345–349 (2012).
4. M. Gersemann, S. Becker, I. Kübler, M. Koslowski, G. Wang, K. R. Herrlinger, J. Griger, P. Fritz, K. Fellermann, M. Schwab, J. Wehkamp, and E. F. Stange, "Differences in goblet cell differentiation between Crohn's disease and ulcerative colitis," Differentiation **77**(1), 84–94 (2009).
5. R. Kiesslich, M. Goetz, K. Lammersdorf, C. Schneider, J. Burg, M. Stolte, M. Vieth, B. Nafe, P. R. Galle, and M. F. Neurath, "Chromoscopy-Guided Endomicroscopy Increases the Diagnostic Yield of Intraepithelial Neoplasia in Ulcerative Colitis," Gastroenterology **132**(3), 874–882 (2007).
6. P. Correa, "Human Gastric Carcinogenesis: A Multistep and Multifactorial Process—First American Cancer Society Award Lecture on Cancer Epidemiology and Prevention," Cancer Res. **52**, 6735–6740 (1992).
7. P. Correa, B. M. Piazuelo, and K. T. Wilson, "Pathology of Gastric Intestinal Metaplasia: Clinical Implications," Am. J. Gastroenterol. **105**(3), 493–498 (2010).
8. H. Bao, A. Boussioutas, J. Reynolds, S. Russell, and M. Gu, "Imaging of goblet cells as a marker for intestinal metaplasia of the stomach by one-photon and two-photon fluorescence endomicroscopy," J. Biomed. Opt. **14**(6), 064031 (2009).
9. R. Kiesslich, L. Gossner, M. Goetz, A. Dahlmann, M. Vieth, M. Stolte, A. Hoffman, M. Jung, B. Nafe, P. R. Galle, and M. F. Neurath, "In Vivo Histology of Barrett's Esophagus and Associated Neoplasia by Confocal Laser Endomicroscopy," Clin. Gastroenterol. Hepatol. **4**(8), 979–987 (2006).
10. X. Li, H. Li, X. He, T. Chen, X. Xia, C. Yang, and W. Zheng, "Spectrum- and time-resolved endogenous multiphoton signals reveal quantitative differentiation of premalignant and malignant gastric mucosa," Biomed. Opt. Express **9**(2), 453–471 (2018).
11. T. Matsui, H. Mizuno, T. Sudo, J. Kikuta, N. Haraguchi, J.-I. Ikeda, T. Mizushima, H. Yamamoto, E. Morii, M. Mori, and M. Ishii, "Non-labeling multiphoton excitation microscopy as a novel diagnostic tool for discriminating normal tissue and colorectal cancer lesions," Sci. Rep. **7**(1), 6959 (2017).
12. S. M. Zhuo, G. Z. Wu, J. X. Chen, X. Q. Zhu, and S. S. Xie, "Label-free imaging of goblet cells as a marker for differentiating colonic polyps by multiphoton microscopy," Laser Phys. Lett. **9**(6), 465–468 (2012).

Biomedical Optics EXPRESS

13. A. Aguirre, Y. Chen, B. Bryan, H. Mashimo, Q. Huang, J. Connolly, and J. Fujimoto, "Cellular resolution ex vivo imaging of gastrointestinal tissues with optical coherence microscopy," J. Biomed. Opt. **15**(1), 016025 (2010).
14. A. D. Aguirre, J. Sawinski, S.-W. Huang, C. Zhou, W. Denk, and J. G. Fujimoto, "High speed optical coherence microscopy with autofocus adjustment and a miniaturized endoscopic imaging probe," Opt. Express **18**(5), 4222–4239 (2010).
15. Y. Chen, S.-W. Huang, A. D. Aguirre, and J. G. Fujimoto, "High-resolution line-scanning optical coherence microscopy," Opt. Lett. **32**(14), 1971–1973 (2007).
16. D. Kang, S. C. Schlachter, R. W. Carruth, M. Kim, T. Wu, N. Tabatabaei, A. R. Soomro, C. N. Grant, M. Rosenberg, N. S. Nishioka, and G. J. Tearney, "Large-area spectrally encoded confocal endomicroscopy of the human esophagus in vivo," Lasers Surg. Med. **49**(3), 233–239 (2017).
17. D. Kang, M. Suter, C. Boudoux, P. Yachimski, B. Bouma, N. Nishioka, and G. Tearney, Combined spectrally encoded confocal microscopy and optical frequency domain imaging system, Proc. SPIE (2009), Vol. 7172.
18. D. Kang, M. J. Suter, C. Boudoux, H. Yoo, P. S. Yachimski, W. P. Puricelli, N. S. Nishioka, M. Mino-Kenudson, G. Y. Lauwers, B. E. Bouma, and G. J. Tearney, "Comprehensive imaging of gastroesophageal biopsy samples by spectrally encoded confocal microscopy," Gastrointest. Endosc. **71**(1), 35–43 (2010).
19. X. Yu, Y. Luo, X. Liu, S. Chen, X. Wang, S. Chen, and L. Liu, "Toward High-Speed Imaging of Cellular Structures in Rat Colon Using Micro-optical Coherence Tomography," IEEE Photonics J. **8**, 1–8 (2016).
20. S. Lee, J. H. Lee, T. Wang, W. H. Jang, Y. Yoon, B. Kim, Y. W. Jun, M. J. Kim, and K. H. Kim, "Three-photon tissue imaging using moxifloxacin," Sci. Rep. **8**(1), 9415 (2018).
21. S. Lee, W. Y. Park, H. Chang, B. Kim, W. H. Jang, S. Kim, Y. Shin, M. J. Kim, K. H. Lee, E. H. Kim, E. Chung, and K. H. Kim, "Fast and sensitive delineation of brain tumor with clinically compatible moxifloxacin labeling and confocal microscopy," J. Biophotonics **13**, e201900197 (2020).
22. T. Wang, W. H. Jang, S. Lee, C. J. Yoon, J. H. Lee, B. Kim, S. Hwang, C.-P. Hong, Y. Yoon, G. Lee, V.-H. Le, S. Bok, G. O. Ahn, J. Lee, Y. S. Gho, E. Chung, S. Kim, M. H. Jang, S.-J. Myung, M. J. Kim, P. T. C. So, and K. H. Kim, "Moxifloxacin: Clinically compatible contrast agent for multiphoton imaging," Sci. Rep. **6**(1), 27142 (2016).
23. J. A. Ocaña, F. J. Barragán, and M. Callejón, "Spectrofluorimetric determination of moxifloxacin in tablets, human urine and serum," Analyst **125**(12), 2322–2325 (2000).
24. S. M. Robertson, M. A. Curtis, B. A. Schlech, A. Rusinko, G. R. Owen, O. Dembinska, J. Liao, and D. C. Dahlin, "Ocular Pharmacokinetics of Moxifloxacin After Topical Treatment of Animals and Humans," Surv. Ophthalmol. **50**(6), S32–S45 (2005).
25. W. H. Jang, A. Park, T. Wang, C. J. Kim, H. Chang, B.-G. Yang, M. J. Kim, S.-J. Myung, S.-H. Im, M. H. Jang, Y.-M. Kim, and K. H. Kim, "Two-photon microscopy of Paneth cells in the small intestine of live mice," Sci. Rep. **8**(1), 14174 (2018).
26. S. Kim, S. Lee, H. Chang, M. Kim, M. J. Kim, and K. H. Kim, "In vivo fluorescence imaging of conjunctival goblet cells," Sci. Rep. **9**(1), 15457 (2019).
27. X. Liu, L. Zhang, M. Kirby, R. Becker, S. Qi, and F. Zhao, "Iterative l1-min algorithm for fixed pattern noise removal in fiber-bundle-based endoscopic imaging," J. Opt. Soc. Am. **33**(4), 630–636 (2016).
28. B. Chassaing, J. D. Aitken, M. Malleshappa, and M. Vijay-Kumar, "Dextran Sulfate Sodium (DSS)-Induced Colitis in Mice," Curr. Protoc. Immunol. **104**, 15.25.11–15.25.14 (2014).
29. M. Shinoda, M. Shin-Ya, Y. Naito, T. Kishida, R. Ito, N. Suzuki, H. Yasuda, J. Sakagami, J. Imanishi, K. Kataoka, O. Mazda, and T. Yoshikawa, "Early-stage blocking of Notch signaling inhibits the depletion of goblet cells in dextran sodium sulfate-induced colitis in mice," J. Gastroenterol. **45**(6), 608–617 (2010).
30. P. Ramakrishnan, M. Maclean, S. J. MacGregor, J. G. Anderson, and M. H. Grant, "Cytotoxic responses to 405 nm light exposure in mammalian and bacterial cells: Involvement of reactive oxygen species," Toxicol. In Vitro **33**, 54–62 (2016).